Combustion and Flame 267 (2024) 113563

Contents lists available at ScienceDirect

Combustion and Flame

journal homepage: www.sciencedirect.com/journal/combustion-and-flame

A consistent explanation of seemingly inconsistent experimental and theoretical data for $N_2O + O$ via MultiScale Informatics

Joe Lee [a], Mark C. Barbet [a], Carly E. LaGrotta [a], Qinghui Meng [a], Lei Lei [a], Francis M. Haas [b], Michael P. Burke [a,c,d,*]

[a] Department of Mechanical Engineering, Columbia University, New York, NY, 10027, USA
[b] Department of Mechanical Engineering, Rowan University, Glassboro, NJ, 08028, USA
[c] Department of Chemical Engineering, Columbia University, New York, NY, 10027, USA
[d] Data Science Institute, Columbia University, New York, NY, 10027, USA

ARTICLE INFO

Keywords:
NO_x formation
N_2O mechanism
Kinetic modeling
Uncertainty quantification

ABSTRACT

The $N_2O + O$ reaction plays a critical role in NO_x formation at high pressures and low peak temperatures, in the "dark zone" region of deflagration waves of organic energetic materials, and in N_2O consumption in NH_3 combustion. While the rate constant for $N_2O + O = NO + NO$ (R3) is considered reasonably well established, viewpoints regarding the rate constants for $N_2O + O = N_2 + O_2$ (R2)—and even the main products of the $N_2O + O$ reaction—have not reached a consensus, with studies from the past few years continuing to reach drastically different conclusions. To date, no single model has been presented that can reproduce all key datasets on *both* sides of the debate. Using the MultiScale Informatics (MSI) approach, we identified a model consistent with a vast catalog of theoretical and experimental data previously used to determine rate constants for R2, R3, and other key reactions influencing experimental interpretations. Notably, this MSI model (presented herein) reproduces all experimental datasets previously used to anchor low-activation-energy k_2 expressions that greatly favor R2 at intermediate temperatures. However, its kinetic parameters are also consistent with theoretical calculations that instead show high activation energy for R2 and k_2 values many orders of magnitude lower—such that R3 is the main channel at essentially all temperatures. This model is also consistent with our new experimental data (presented in our companion paper) at optimally selected conditions that avoid the interpretation ambiguities that have hindered definitive conclusions from previous experimental data. The present analysis elucidates the role of secondary reactions that would have artificially inflated the apparent k_2/k_3 ratio previously deduced from experiments in a manner that may not have been detectable from even multi-species measurements at typical conditions—and may, therefore, explain the persistent historical difficulties in establishing the main products of $N_2O + O$.

Novelty and significance statement

Despite decades of research, viewpoints regarding the rate constants for $N_2O + O = N_2 + O_2$ (R2)—and even the main products of the $N_2O + O$ reaction—have not reached a consensus, with studies from the past few years still reaching drastically different conclusions. To date, no single model has been presented that can reproduce all key datasets on *both* sides of the debate. Here, we present a single model consistent with a vast catalog of theoretical and experimental data, including all experimental datasets previously used to anchor low-activation-energy expressions for k_2 that greatly favor R2 as the main channel at intermediate temperatures—but with kinetic parameters consistent with theoretical calculations that instead show high activation energy for R2 and $N_2O + O = NO + NO$ (R3) as the main channel at essentially all temperatures.

1. Introduction

Together with

$$N_2O\ (+M) \rightleftharpoons N_2 + O\ (+M) \quad \text{(R1)}$$

the reaction of N_2O with O

$$N_2O + O \rightleftharpoons N_2 + O_2 \quad \text{(R2)}$$

* Corresponding author at: Department of Mechanical Engineering, Columbia University, New York, NY, 10027, USA.
E-mail address: mpburke@columbia.edu (M.P. Burke).

https://doi.org/10.1016/j.combustflame.2024.113563
Received 18 January 2024; Received in revised form 4 June 2024; Accepted 4 June 2024

$N_2O + O \rightleftharpoons NO + NO$ (R3)

plays a key role in NO_x formation at high pressures and low peak temperatures [1–3], in the "dark zone" region of deflagration waves of organic energetic materials [4,5], and in N_2O consumption in NH_3 combustion [6]. Species measurements during N_2O decomposition experiments have often been used as a way to infer the rate parameters for (R1)–(R3) from simpler chemical systems than those of combustion.

The rate constant for (R1), which is the initiating reaction and main rate-limiting step in N_2O decomposition, is relatively well established for common bath gases at 1 atm (with remaining uncertainties due to crossing seam anharmonicity [7], tunneling [8], third-body efficiencies [6,9,10], and mixture rules [11–13]). Likewise, the rate constant for (R3), for which the rate constant for the reverse reaction can also be determined from experiments with NO as the reactant, is also relatively well established [6,14] and experimental determinations agree with *ab initio* theoretical kinetics calculations [15,16].

However, despite decades of research, viewpoints regarding the rate constants for (R2)—and even the main products of the $N_2O + O$ reaction—have not reached a consensus, with studies from the past few years continuing to reach drastically different conclusions [6,16,17]. To make matters worse, contradictory conclusions have been reached for every class of study, with some theoretical studies [15], experimental studies [18], and review studies [6] each reaching entirely different conclusions from others [14,16,17], as described in the following paragraphs.

The earliest studies (e.g., [18]), which relied on indirect inferences from experimental data, led to the first long-prevailing notion summarized in several review studies that $k_2 \approx k_3$ (i.e., $k_2 / k_3 \approx 1$) for all temperatures with an activation energy of ~28 kcal/mol [19–22].

This view largely prevailed until the landmark experimental study in 1992 by Davidson et al. [23], who used their measured O_2 and NO time profiles in shock-heated N_2O/Ar mixtures to infer k_2 and k_3, respectively, using a detailed kinetic mechanism. While their k_3 determinations agreed with previous and later work, their k_2 determinations indicated a much lower pre-exponential factor and activation energy (~10.8 kcal/mol) than previously thought [19,20].

This newer view [23] was strengthened by the equally influential review in 2000 by Meagher and Anderson [14], who critically evaluated dozens of previous studies using detailed kinetic modeling. Their analysis led them to discard essentially all previous data for k_2 due to experimental and/or interpretive artifacts (low-purity gases, H_2O contamination, surface reactions, boundary layer effects, thermal equilibrium issues, etc.) except for those from two studies: (1) Davidson et al. [23] (discussed above) and (2) Fontijn et al. [24] (the experimental companion study to [14]). Fontijn et al. used their measured O time profiles in flash-photolyzed N_2O/precursor/Ar mixtures to derive $k_2 + k_3$ at intermediate temperatures. Given that their derived $k_2 + k_3$ values were much greater than previously established values for k_3, $k_2 + k_3$ was primarily attributed to k_2—suggesting much higher k_2 and k_2/k_3 (favoring $N_2 + O_2$) at intermediate temperatures than the earliest studies [20] but agreeing with the low pre-exponential factor and activation energy suggested by Davidson et al. [23]. These two studies [23,24] formed the sole basis for the k_2 recommendation in Meagher and Anderson [14].

A year later, González et al. [15] calculated rate constants for both (R2) and (R3) via the triplet surface using *ab initio* transition state theory. While their calculations agreed with previous data for (R3), they showed a very high barrier for (R2) (~40 kcal/mol)—yielding much lower k_2 and implying NO + NO as the dominant products at most temperatures. Interestingly, there were contemporary experimental studies providing support for the lower ranges of k_2. Using measured O time profiles measurements in shock-heated N_2O/Ar mixtures, Ross et al. [25] inferred an upper limit for $k_2 + k_3$ similar to (though disconcertingly somewhat lower than) previously established values of k_3—implying an upper limit for k_2 inconsistent with the higher proposed ranges [14,23].

In spite of these two studies [15,25], kinetic models [26–33] (with few exceptions [22,34]) have generally adopted rate constants [14,23] with low pre-exponential factor and low activation energy. That is, the modern prevailing view is that $N_2 + O_2$ are the main products of $N_2O + O$ at intermediate temperatures.

In fact, the recent experimental and theoretical studies by Pham, Lin, and co-workers [16,17] (in 2020 and 2022) appear to provide further support for very high k_2. Their inferred values of k_2 from their measured NO time profiles in N_2O/Ar mixtures and theoretically calculated values of k_2 via intersystem crossing (ISC) are even a factor of ~5 higher at 1000 K than the recommendation of Meagher and Anderson [14].

Just a few months ago, however, Glarborg et al. [6] presented the most recent critical evaluation of previous studies using detailed kinetic modeling. They showed (consistent with the present work) that the measured NO time profiles from Pham et al. [17] can be equally well reproduced using the very low k_2 indicated by the earlier theoretical calculations on the triplet surface of González et al. [15]. They also point out that the reported geometry [16] of the ISC point, which is central to the ISC calculations of Pham and Lin [16], does not actually satisfy the requirement that the singlet and triplet energies at the ISC point have to be equal. Calculations using CCSD/aug-cc-pVTZ theory (as used in [16]) of the triplet and singlet energies at the ISC geometry are 11 and 33 kcal/mol, respectively—indicating an error in the ISC calculations [6].

Glarborg et al. [6] advocated that $k_2 \approx 0$, for which the primary support appears to come from their interpretations of Zuev and Starikovskii [35], which Meagher and Anderson [14] discarded due to experimental artifacts (boundary layer growth and heat release), Kaufman et al. [18], which Meagher and Anderson [14] discarded due to experimental artifacts (surface reactions and thermal equilibrium issues), and Ross et al. [25], for which their modeling [6] employed an unexplained adjustment in k_1 by a factor of two. Notably, Glarborg et al. [6] do not show comparisons of their model against the data from Fontijn et al. [24] and their model does not reproduce the data of Davidson et al. [23]—i.e., the two datasets on which Meagher and Anderson [14] anchor their recommendations.

In other words, the two most comprehensive and recent reviews of the title reaction [6,14] reach opposite conclusions on the basis of entirely different sets of data. All told, with such frustratingly opposite viewpoints among theoretical [15,16], experimental [17,18], and review [6,14] studies, it is clearly difficult to come to any satisfying conclusion regarding the value of k_2 and even whether $N_2 + O_2$ or NO + NO are the main reaction products at intermediate temperatures.

At the heart of the issue is the fact that any individual rate constants derived using an assumed kinetic model—even for a deceivingly simple mechanism—will depend on the parameters assumed for the other reactions. This complication was noted by Allen et al. [36], who found that even their simultaneous measurements of four species (N_2O, O_2, NO, and NO_2) could be reproduced equally well with models using drastically different k_2 [20,23] with only 30% differences in k_1 (which is well below estimated uncertainties in k_1). Yet, no previous analysis of experimental data for k_2 and k_3, including all reviews before [19–21] and after [6,14,29] the study of Allen et al. [36], simultaneously considered species measurements used to constrain k_1.

A further confounding factor is the role of the secondary reactions [6,14,36]

$NO + O (+M) \rightleftharpoons NO_2 (+M)$ (R4)

$NO_2 + O \rightleftharpoons NO + O_2$ (R5)

which, as we describe herein, would lead to artificially high k_2/k_3 if data are interpreted in their absence or, interestingly, if larger values of k_2 are used when assessing their impact.

All of this implies that reanalysis of previous experimental data requires simultaneous consideration of datasets used to inform multiple

Table 1
List of parameters used in the optimization[a].

Reaction		Kinetic parameters	Source
(R1)	N_2O (+M) = N_2 + O (+M)	A'_{R1} n_{R1} $E_{a,R1}$	[22]
(R2)	N_2O + O = N_2 + O_2	$E_{B1,R2}$ $\nu'_{B1,R2}$ $\nu'_{imag\,B1,R2}$ $E_{B2,R2}$ $\nu'_{B2,R2}$ $\nu'_{imag\,B2,R2}$	[15]
(R3)	N_2O + O = NO + NO	$E_{B1,R3}$ $\nu'_{B1,R3}$ $\nu'_{imag\,B1,R3}$ $E_{B2,R3}$ $\nu'_{B2,R3}$ $\nu'_{imag\,B2,R3}$	
(R4)	NO + O (+M) = NO_2 (+M)	A'_{R4} n_{R4} $E_{a,R4}$	[22]
(R5)	NO_2 + O = NO + O_2	A'_{R5} $E_{a,R5}$	[41]
Macroscopic observables		Physical model parameters	Source
e = 1, 2	Flow reactor: $N_2O/H_2O/N_2$	T'_e P'_e Δt_e $X'_{N_2O,t=0,e}$ $X'_{H_2O,t=0,e}$ $X'_{N_2,t=0,e}$	[36]
e = 3...90	Jet-Stirred reactor: N_2O/NO/NO_2/He	T'_e P'_e τ'_e $X'_{N_2O,in,e}$ $X'_{NO,in,e}$ $X'_{NO_2,in,e}$ $X'_{He,in,e}$	[37]
e = 91, 92	Shock tube: N_2O/Ar	T'_e P'_e Δt_e $X'_{N_2O,t=0,e}$ $X'_{Ar,t=0,e}$	[23]
e = 93, 94	Flow reactor: N_2O/H_2O/Ar	T'_e P'_e τ'_e $X'_{N_2O,in,e}$ $X'_{H_2O,in,e}$ $X'_{Ar,in,e}$	[42]
e = 95	Flow reactor: N_2O/Ar	T'_e P'_e Δt_e $X'_{N_2O,t=0,e}$ $X'_{Ar,t=0,e}$	[43]
e = 96	Flow reactor: N_2O/H_2O/Ar	T'_e P'_e τ'_e $X'_{N_2O,in,e}$ $X'_{H_2O,in,e}$ $X'_{Ar,in,e}$	[44]
e = 97	Flow reactor: N_2O/H_2O/He	T'_e P'_e τ'_e $X'_{N_2O,in,e}$ $X'_{H_2O,in,e}$ $X'_{He,in,e}$	
e = 98	Flow reactor: $N_2O/H_2O/N_2$	T'_e P'_e τ'_e $X'_{N_2O,in,e}$ $X'_{H_2O,in,e}$ $X'_{N_2,in,e}$	
e = 99...113	Shock tube: N_2O/Ar	T'_e P'_e Δt_e $X'_{N_2O,t=0,e}$ $X'_{Ar,t=0,e}$	[45]
e = 114, 115	Static reactor: N_2O/Ar	T'_e P'_e $X'_{N_2O,t=0,e}$ $X'_{Ar,t=0,e}$	[17]
e = 116...118	Shock tube: N_2O/Ar	T'_e P'_e Δt_e $X'_{N_2O,t=0,e}$ $X'_{Ar,t=0,e}$ $\hat{\sigma}'_O$	[25]

[a] Note that $'$ indicates the natural logarithm of the quantity relative to the (nominal) value in the *a priori* model.

reactions, including not only (R2) and/or (R3) but also (R1) and others such as (R4) and (R5). Furthermore, any definitive conclusions regarding k_2 would also require new intermediate-temperature experiments that can constrain k_2 more effectively than previous experiments.

The present paper and our companion paper address these two needs. Our companion paper [37] presents new experiments at optimally selected conditions that avoid the interpretation ambiguities that have hindered previous conclusions based solely on experimental data. This paper presents a comprehensive analysis of previous data for all five important reactions ((R1)–(R5)) using our MultiScale Informatics (MSI) approach [38–40], which has previously enabled identification of consistent (and reliable [38]) explanations of apparently inconsistent data. This analysis focuses on the theoretical calculations of González et al. [15] based on the issues with the calculations of Pham and Lin [16] raised by Glarborg et al. [6] and based on our own experiments [37], which convincingly rule out such high values of k_2. We show that the resulting MSI model—notably with a high activation energy consistent with [15]—is broadly consistent with both theoretical data and experimental data across a broad array of experimental conditions, including measurements used to constrain k_1 across wide ranges of temperature, our new intermediate-temperature measurements [37], and, importantly, measurements from Davidson et al. [23], Fontijn et al. [24], and Pham et al. [17] that previously anchored the low-activation-energy k_2 expressions [14,16,23].

2. Approach

In short, the MSI approach [38] identifies optimized values and quantified uncertainties for a set of molecular parameters (within theoretical kinetics calculations), rate parameters, and physical model parameters (within simulations of experimental observables) informed by data from various sources and scales. Theoretical kinetics calculations (e.g., TST, RRKM-ME) relate active molecular parameters (e.g., barrier heights) to rate constants for phenomenological reactions. Kinetic models, consisting of these rate constants for some reactions and any active rate parameters for other reactions (e.g., pre-exponential factors or activation energies) are then combined with physical models (e.g., adiabatic, constant-volume reactors) and active physical model parameters (e.g., initial temperatures) for each experiment to predict macroscopic observables measured experimentally. These multiscale, physics-based models enable predictions, $f_i(\boldsymbol{x})$, for a given set of active parameters, $\boldsymbol{x}$, of properties spanning molecular to macroscopic scales.

Inverse uncertainty quantification (UQ) [46] is then accomplished via a surrogate-model-based minimization of the uncertainty-weighted least-squares error between model predictions of the ith target, $f_i(\boldsymbol{x})$, and the target datum, y_i^t,

$$E(\boldsymbol{x}) = \sum \left(\frac{y_i^t - f_i(\boldsymbol{x})}{z_i} \right)^2 \quad (1)$$

where the weighting factor, z_i, is equal to the uncertainty of the ith target datum, σ_i, divided by an additional weighting factor, $w_i = n^{-0.5}$, where n is the number of data points in the dataset from a particular study. Assuming multivariate normal prior and posterior distributions and local linearity near the optimized values (similar to other inverse UQ studies of comparable size [46–48]), the joint probability distribution function of the MSI model (i.e., the posterior) is then described by the optimized set of active parameters, $\boldsymbol{x}^*$, and covariance matrix, $\boldsymbol{\Sigma}$. Uncertainties here are intended to correspond to two standard deviations.

In the results shown below, the *a priori* model consists of all parameters at their nominal values with uncertainties constrained only by *ab initio* calculated values for molecular parameters, reported experimental conditions for physical model parameters, and other priors; the (optimized) MSI model consists of all optimized parameters with uncertainties additionally constrained by rate constant determinations and/or measured macroscopic observables; and prediction uncertainties were propagated using the covariance matrix.

3. Implementation

The MSI analysis focused on the five reactions (cf. Table 1) relevant to interpreting the raw data from the key experiments. The *a priori* model used rate constants from the theoretical calculations of González et al. [15] for (R2) and (R3); recently proposed rate constants for (R5) [41]; rate constants for (R1) and (R4) from Glarborg et al. [22] (with third-body efficiencies readjusted to match the original data on which the efficiencies in [22] were based, shown in Fig. 2 and S2–S4, yielding values of ε_{H_2O} = 15.0, ε_{He} = 2.7, ε_{N_2} = 2.1, and ε_{O_2} = 2.2 for (R1)); and rate constants for the H/N/O reactions of secondary

Table 2
List of targets used in the optimization[a,b].

I. *Ab Initio* calculations			Source
	$E_{B1,R2}$(5 kcal mol^{-1}) $\nu'_{B1,R2}$(0.22) $\nu'_{imag\,B1,R2}$(0.26) $E_{B2,R2}$(5 kcal mol^{-1}) $\nu'_{B2,R2}$(0.22) $\nu'_{imag\,B2,R2}$(0.26)		[15]
	$E_{B1,R3}$(5 kcal mol^{-1}) $\nu'_{B1,R3}$(0.22) $\nu'_{imag\,B1,R3}$(0.26) $E_{B2,R3}$(5 kcal mol^{-1}) $\nu'_{B2,R3}$(0.22) $\nu'_{imag\,B2,R3}$(0.26)		
II. Rate constant measurements			Source
	k_4(0.69 − 1.61)		[49,50]
	III. Global experiments	IV. Experimental conditions	Source
e = 1, 2	$X'_{N_2O,t,e}$(0.1) $X'_{NO,t,e}$(0.07 − 0.2) $X'_{NO_2,t,e}$(0.1 − 0.2) $X'_{O_2,t,e}$(0.09 − 0.3)	T'_e(0.003) P'_e(0.02) Δt_e(0.4 s) $X'_{N_2O,t=0,e}$(0.03) $X'_{H_2O,t=0,e}$(0.1) $X'_{N_2,t=0,e}$(0.03)	[36]
e = 3...90	$X'_{N_2O,out,e}$(0.1) $X'_{NO,out,e}$(0.05 − 0.09) $X'_{NO_2,out,e}$(0.09 − 5000) $X'_{O_2,out,e}$(0.05 − 0.09) $X'_{N_2,out,e}$(0.05 − 0.09)	T'_e(0.01) P'_e(0.01) τ'_e(0.05) $X'_{N_2O,in,e}$(0.008 − 0.06) $X'_{NO,in,e}$(0.02 − 0.05) $X'_{NO_2,in,e}$(0.02 − 0.1) $X'_{He,in,e}$(0.0008 − 0.02)	[37]
e = 91, 92	$X'_{O_2,t,e}$(0.05) $X'_{NO,t,e}$(0.05)	T'_e(0.02) P'_e(0.02) Δt_e(10 μs) $X'_{N_2O,t=0,e}$(0.01) $X'_{Ar,t=0,e}$(0.01)	[23]
e = 93, 94	$X'_{N_2O,out,e}$(0.07 − 0.2)	T'_e(0.01) P'_e(0.02) τ'_e(0.05) $X'_{N_2O,in,e}$(0.02) $X'_{H_2O,in,e}$(0.1) $X'_{Ar,in,e}$(0.02)	[42]
e = 95	$X'_{N_2O,t,e}$(0.05) $X'_{NO,t,e}$(0.1) $X'_{N_2,t,e}$(0.05 − 0.06)	T'_e(0.01) P'_e(0.02) Δt_e(10 s) $X'_{N_2O,t=0,e}$(0.05) $X'_{Ar,t=0,e}$(0.05)	[43]
e = 96	$X'_{N_2O,out,e}$(0.08 − 0.1)	T'_e(0.01) P'_e(0.02) τ'_e(0.05) $X'_{N_2O,in,e}$(0.02) $X'_{H_2O,in,e}$(0.3) $X'_{Ar,in,e}$(0.0001)	[44]
e = 97	$X'_{N_2O,out,e}$(0.08 − 0.5)	T'_e(0.01) P'_e(0.02) τ'_e(0.05) $X'_{N_2O,in,e}$(0.02) $X'_{H_2O,in,e}$(0.3) $X'_{He,in,e}$(0.0001)	
e = 98	$X'_{N_2O,out,e}$(0.07 − 0.2)	T'_e(0.01) P'_e(0.02) τ'_e(0.05) $X'_{N_2O,in,e}$(0.02) $X'_{H_2O,in,e}$(0.3) $X'_{N_2,in,e}$(0.0001)	
e = 99...113	$X'_{N_2O,t,e}$(0.06 − 4)	T'_e(0.02) P'_e(0.04) Δt_e(10 μs) $X'_{N_2O,t=0,e}$(0.1) $X'_{Ar,t=0,e}$(0.1)	[45]
e = 114, 115	$X'_{N_2O,t,e}$(0.07 − 0.2) $X'_{NO,t,e}$(0.1)	T'_e(0.01) P'_e(0.02) $X'_{N_2O,t=0,e}$(0.02) $X'_{Ar,t=0,e}$(0.02)	[17]
e = 116...118	$abs'_{O,t,e}$(0.08 − 2)	T'_e(0.02) P'_e(0.02) Δt_e(10 μs) $X'_{N_2O,t=0,e}$(0.03) $X'_{Ar,t=0,e}$(0.03) $\hat{\sigma}'_O$(0.5)	[25]

[a] Note that $'$ indicates the natural logarithm of the quantity relative to the (nominal) value in the *a priori* model.
[b] Uncertainties listed in () are intended to reflect two standard deviations.

importance (not listed in Table 1) from [22] (with a correction to the third-body efficiency of Ar in O + O + M = O_2 + M from 0 to 1, an issue which may have stemmed from inadvertent omission of a dedicated Arrhenius expression for an Ar bath).

Active kinetic parameters were then assigned to represent the uncertainties in the kinetic model (cf. Table 1). The theoretical kinetics calculations of González et al. [15] were used for the active kinetic treatment of (R2) and (R3). Active parameters were assigned to the barrier height (E), scaling factor for all harmonic frequencies (ν), and scaling factor for the imaginary frequency (ν_{imag}) of each of the two transition states involved in (R2) and (R3) with uncertainties (cf. Table 2) commensurate with the difficulties of CASPT2//CASSCF(18,14) calculations in describing reactions with such large barrier heights.

For (R1), whose rate constant is sufficiently constrained by macroscopic observables across the full range of relevant temperatures here, modified Arrhenius parameters were considered as active parameters (without prior constraints). For (R5), Arrhenius parameters were considered as active parameters with a prior uncertainty of a factor of 10 for the pre-exponential factor and a prior uncertainty of 4 kcal/mol for the activation energy (to represent the uncertainties in the theoretical calculations from Li et al. [41], for which insufficient information was provided in their paper to employ the full theoretical treatment within MSI). For (R4), similar to (R1), modified Arrhenius parameters were considered as active parameters without prior constraints, though rate constant determinations [49,50] were included as targets with conservative uncertainties of a factor of two. (While it would be better to include the raw data [49,50] as macroscopic observables to enable their reinterpretation [38], the raw data used to infer k_4 in those studies [49,50] are not available.) To assess the influence of secondary reactions (i.e., those not listed in Table 1), MSI analysis was performed with and without pre-exponential factors for all other reactions with prior uncertainties from the compilation of Cornell et al. [51], which yielded negligible differences in the results.

Measurements from a wide array of experimental studies used to determine rate constants for (R1)–(R3) were then added as macroscopic observable targets to enable MSI to reinterpret all the data simultaneously. These macroscopic observables included measurements of N_2O, NO, NO_2, O_2, N_2, and O across a wide array of experimental devices (shock tubes, flow reactors, static reactors, and jet-stirred reactors) and temperatures from ~1000 to 2500 K. Measurements with strong signal interference (e.g., absorption by another species) or low signal-to-noise ratio were unweighted in the optimization. The O-atom fluorescence time profiles from Fontijn et al. [24] were not included as target data due to the overwhelming impact of molecular diffusion (but MSI model predictions, shown below, are consistent with the data). In the plots

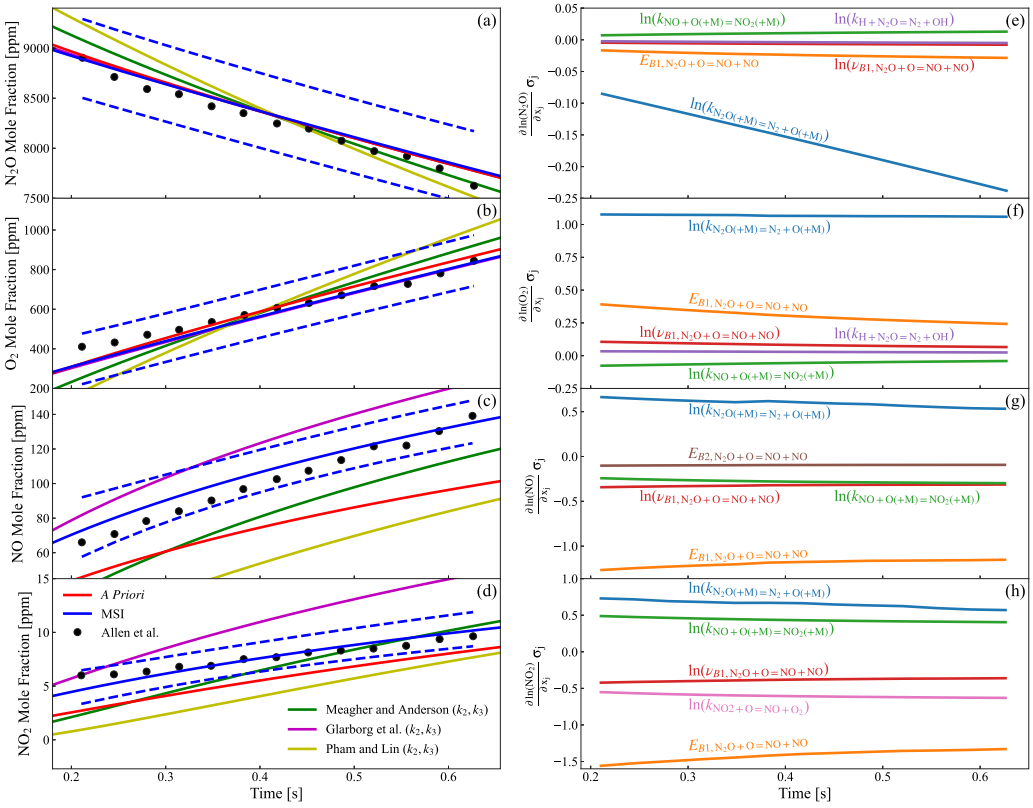

Fig. 1. Time profiles (a–d) and corresponding uncertainty-weighted sensitivity coefficients (e–h) for mole fractions of (a,e) N_2O, (b,f) O_2, (c,g) NO, and (d,h) NO_2 in a flow reactor at 1123 K and 6 atm for an initial mixture of 9640 ppm N_2O, 560 ppm H_2O, and N_2 balance. Symbols denote experimental measurements of Allen et al. [36]; solid lines denote predictions using the *a priori* model, the MSI model, and variants of the *a priori* model that use k_2 and k_3 from Meagher and Anderson [14], Glarborg et al. [22], and Pham and Lin [16]; dashed lines denote the propagated uncertainties in the MSI model predictions. All model predictions are time-shifted to yield the same N_2O mole fraction near the mid-point of N_2O consumption [53].

below, weighted and unweighted data are indicated by closed and open symbols, respectively.

For the time profile measurements (and stirred reactor measurements), the active physical model parameters included the initial (or inlet) reactant mole fractions, temperatures, and pressures (cf. Table 1). The initial time was also considered as an active parameter to account for ambiguities in the start of reaction time such as those due to vibrational non-equilibrium immediately following the shock wave in shock tubes [52] and reactant mixing in some flow reactors [53]. The residence time in other flow reactors was considered as an active parameter to account for noted potential for further reaction in the sampled gases [42,44]. The residence time was also considered as an active parameter in stirred reactor models. In all cases, uncertainties in the macroscopic observables and physical model parameters were based on those reported and/or estimated using typical values.

Macroscopic observables and sensitivity coefficients were generally calculated via standard homogeneous reactor models representative of each experiment (e.g., isochoric/isobaric, adiabatic/isothermal, unmixed/perfectly-mixed) in CANTERA [54]. A notable exception involves the experiments of Mulvihill et al. [45], for which model predictions shown in Fig. 3 and S5–S16 employ the time-varying volume profiles unique to each experiment [45] (as done in [45]). The simulations used for inverse UQ, for simplicity, did not consider the time-varying volume profiles. However, an alternative optimization that excluded experiments for which time-varying volume effects were non-negligible yielded very similar MSI results (with optimized k_1 values within ~10% of the MSI results presented below)—such that it does not appear that neglecting the time-varying volume effects in the MSI optimization negatively impacted the results. In fact, predictions using the MSI model and the time-varying volume profiles agree well with the data.

4. Results and discussion

On the whole, the parameter values and predictions of the MSI model are consistent with the target data from the *ab initio* calculations, rate constant determinations, measured macroscopic observables, and reported experimental conditions—along with other data not included among the target data (e.g., [24]). Of particular interest, this MSI model is consistent with both the theoretical calculations of González et al. [15] *and* the measured macroscopic observables from Davidson et al. [23], Fontijn et al. [24], and Pham et al. [17] that previously anchored the very high proposed k_2 expressions [14,16,23]. This MSI model is also consistent with our new experiments [37], which uniquely exploit NO_2 addition to avoid the interpretation ambiguities for previous experiments.

Below, we present model comparisons against the raw experimental data from studies intended to determine k_1 (Section 4.1) and k_2 and k_3 (Section 4.2). We then compare rate constants for all five key reactions from the *a priori* and MSI models with those originally derived from the data and present further analyses to explain the observed differences in derived k_2 (Section 4.3). Model predictions are shown for the *a priori* model, the MSI model, and variants of the *a priori* model that employ k_2 and k_3 from Glarborg et al. [22], Meagher and Anderson [14], and Pham and Lin [16]. Uncertainty-weighted sensitivity coefficients, $S_{ij}\sigma_j$, for the MSI model predictions are shown for the most influential parameters in the bottom panel of some figures. For context, uncertainty-weighted sensitivity coefficients reflect the uncertainty in the model predictions due to each parameter x_j, and, in turn, indicate which parameters are most relevant to experimental interpretations. The complete list of active parameters, prior uncertainties, and MSI (optimized) values along with additional model comparisons against experimental data are presented in the Supplementary Material.

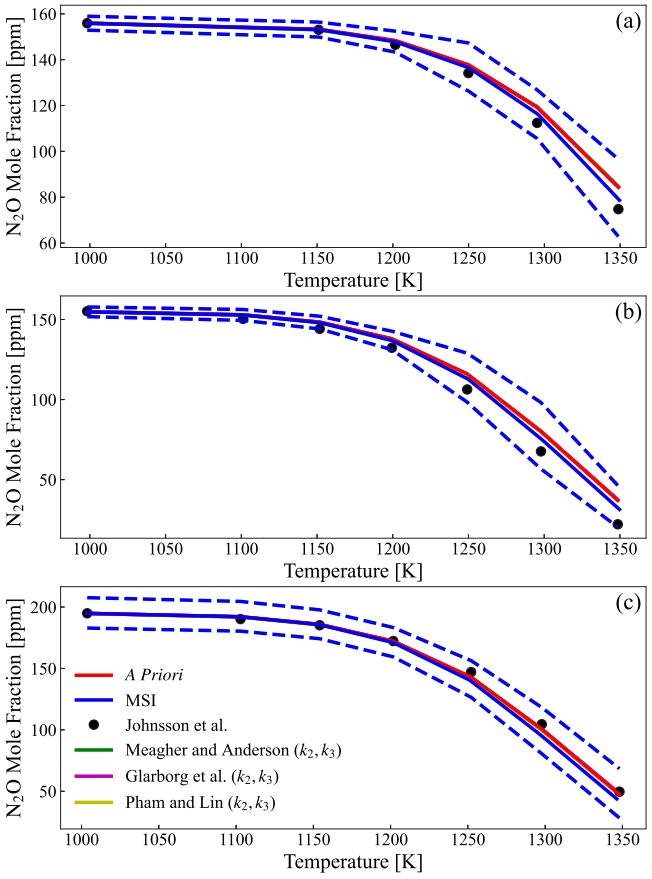

Fig. 2. Outlet N_2O mole fractions from an atmospheric-pressure flow reactor of varied temperature for inlet mixtures of (a) 156 ppm N_2O, ~30 ppm H_2O, and Ar balance; (b) 155 ppm N_2O, ~30 ppm H_2O, and He balance; (c) 195 ppm N_2O, ~30 ppm H_2O, and N_2 balance. Symbols denote experimental measurements of Johnsson et al. [44]; solid lines denote predictions using the *a priori* model, the MSI model, and variants of the *a priori* model that use k_2 and k_3 from [14,16,22]; dashed lines denote the propagated uncertainties in the MSI model predictions. (Note that the predictions using the *a priori* model and its variants with different k_2 and k_3 are essentially indistinguishable).

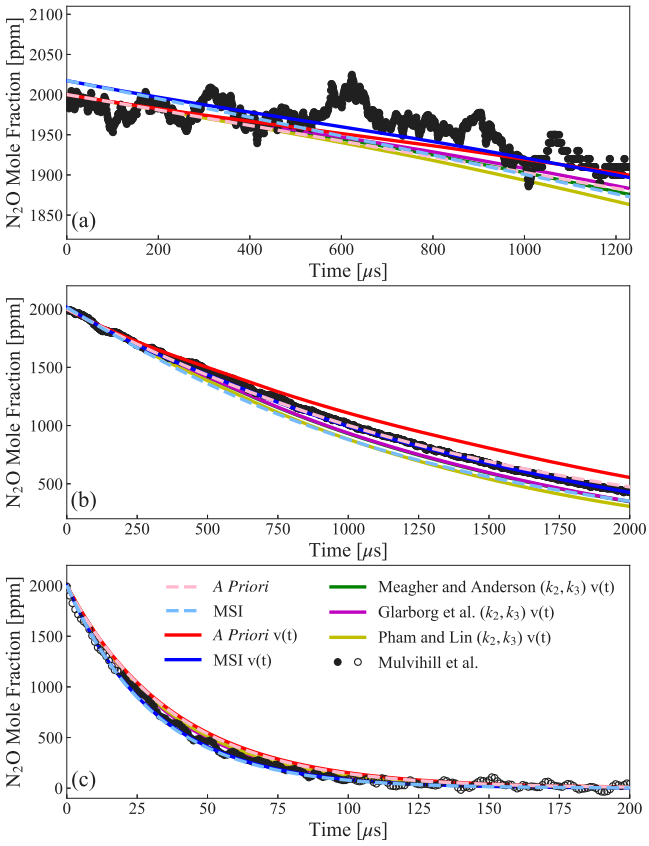

Fig. 3. N_2O time profiles in a shock tube with initial mixtures of 0.2% N_2O and Ar balance at (a) 1546 K and 1.43 atm, (b) 1821 K and 1.31 atm, and (c) 2476 K and 1.08 atm. Symbols denote experimental measurements of Mulvihill et al. [45]; solid lines denote predictions using the *a priori* model, the MSI model, and variants of the *a priori* model that use k_2 and k_3 from [14,16,22] using the time-varying volume profiles for each experiment [45]; dashed lines denote predictions that do not account for the time-varying volume profiles (for comparison).

4.1. Experiments previously used to determine k_1

Model predictions are compared with the raw data from several studies originally used to determine k_1 in Figs. 1–6 and S1–S16, including time profiles of: N_2O, O_2, NO, and NO_2 mole fractions from flow reactor experiments of $N_2O/H_2O/N_2$ mixtures from Allen et al. [36] in Fig. 1 and S1, N_2O mole fractions from flow reactor experiments of N_2O/H_2O/diluent mixtures from Johnsson et al. [44] in Fig. 2 (and analogous experiments from Glarborg et al. [42] in Fig. S2), O atomic resonance absorption spectrophotometry (ARAS) signals from shock tube experiments of N_2O/Ar mixtures from Ross et al. [25] in Figs. 4–5, N_2O mole fractions from shock tube experiments of N_2O/Ar mixtures from Mulvihill et al. [45] in Fig. 3 and S5–S16, and N_2O mole fractions from static reactor experiments of N_2O/Ar mixtures from Pham et al. [17] in Fig. 6. While not originally used to determine k_1, the N_2O, N_2, and NO mole fractions from flow reactor experiments of N_2O/Ar mixtures from Haas et al. [43] (Fig. 11) are also pertinent to this discussion. Several key themes are apparent from these figures.

First, comparison of the *a priori* model variants, which differ only in k_2 and k_3, illustrate (consistent with Allen et al. [36]) that even determination of k_1 is often dependent on the values for k_2 and k_3—which demonstrate the need to consider experimental studies for all three reactions simultaneously. Given that (R2) and (R3) also contribute to N_2O consumption, the predicted rates of N_2O disappearance are consistently higher for models with higher $k_2 + k_3$ (from *a priori* to 'Glarborg et al.' to 'Meagher and Anderson' to 'Pham and Lin' in increasing order). Likewise, given that (R2) and (R3) contribute to O consumption, predicted O mole fractions are consistently lower for models with higher $k_2 + k_3$ (from *a priori* to 'Glarborg et al.' to 'Meagher and Anderson' to 'Pham and Lin' in increasing order). The effect of $k_2 + k_3$ on N_2O disappearance is least noticeable for the N_2O/H_2O/diluent mixtures in flow reactors by Johnsson et al. [44] in Fig. 2 and Glarborg et al. [42] in Fig. S2 (which have the largest H_2O to N_2O ratio among the datasets and therefore encourage O consumption via other reactions). Furthermore, for sufficiently low $k_2 + k_3$ values (e.g., *a priori* and 'Glarborg et al.'), the effect of $k_2 + k_3$ is minimal for the lower-temperature experiments (Allen et al. [36] in Fig. 1 and S1, Pham et al. [17] in Fig. 6, and Haas et al. [43] in Fig. 11).

Second, model variants with higher $k_2 + k_3$ are generally in worse agreement with the measured N_2O mole fractions. This would suggest, at the very least, that the very high values of $k_2 + k_3$ are incompatible with the *a priori* k_1. Since model variants with higher $k_2 + k_3$ tend to predict faster rates of disappearance than observed, the agreement could be improved by a lower k_1—but only in some cases. For example, the N_2O measurements of Johnsson et al. [44] in Fig. 2 and Glarborg et al. [42] in Fig. S2, for which predictions are insensitive to $k_2 + k_3$, would, if anything, imply that k_1 is larger than the *a priori* value.

Third, the MSI model predictions are consistent with the measured rates of N_2O disappearance and O appearance within reasonable uncertainties, exhibiting similar agreement as the *a priori* model for some

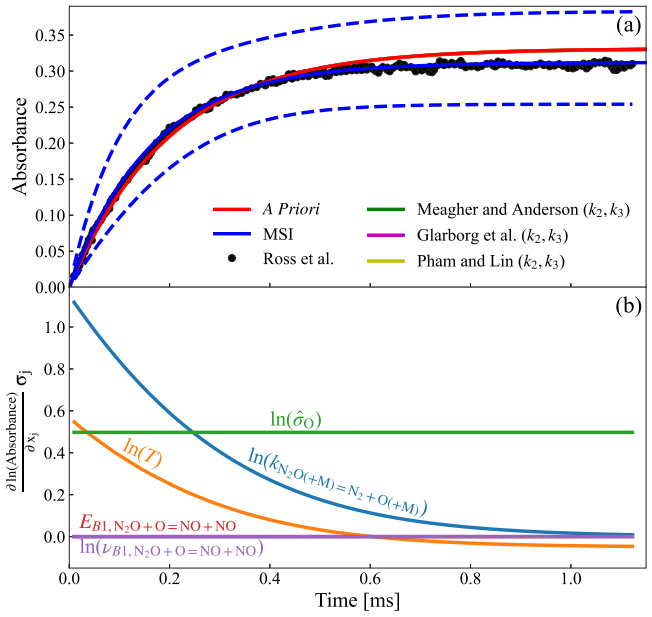

Fig. 4. (a) Time profiles and (b) corresponding uncertainty-weighted sensitivity coefficients for O-ARAS signals in a shock tube at 2163 K and 0.9785 atm with an initial mixture of 2.727 ppm N_2O and Ar balance. Symbols denote experimental measurements of Ross et al. [25]; solid lines denote predictions using the *a priori* model, the MSI model, and variants of the *a priori* model that use k_2 and k_3 from [14,16,22]; dashed lines denote the propagated uncertainties in the MSI model predictions. (Note that the predictions using the *a priori* model and its variants with different k_2 and k_3 are essentially indistinguishable).

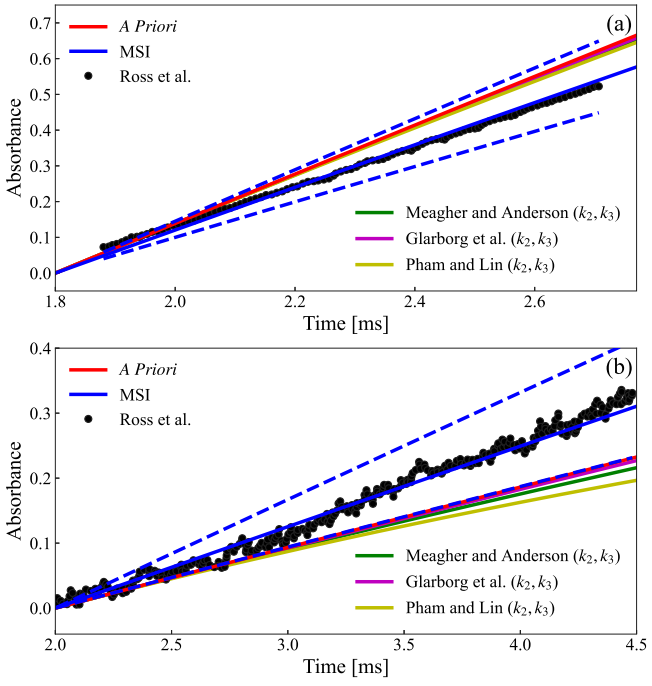

Fig. 5. Time profiles for O-ARAS signals in a shock tube at (a) 1557 K and 0.6259 atm with an initial mixture of 262.5 ppm N_2O and Ar balance, and (b) 1260 K and 0.8627 atm with an initial mixture of 992.5 ppm N_2O and Ar balance. Symbols denote experimental measurements of Ross et al. [25]; solid lines denote predictions using the *a priori* model, the MSI model, and variants of the *a priori* model that use k_2 and k_3 from [14,16,22]; dashed lines denote the propagated uncertainties in the MSI model predictions. (Note that the predictions using the *a priori* model and its variants with different k_2 and k_3 are nearly indistinguishable).

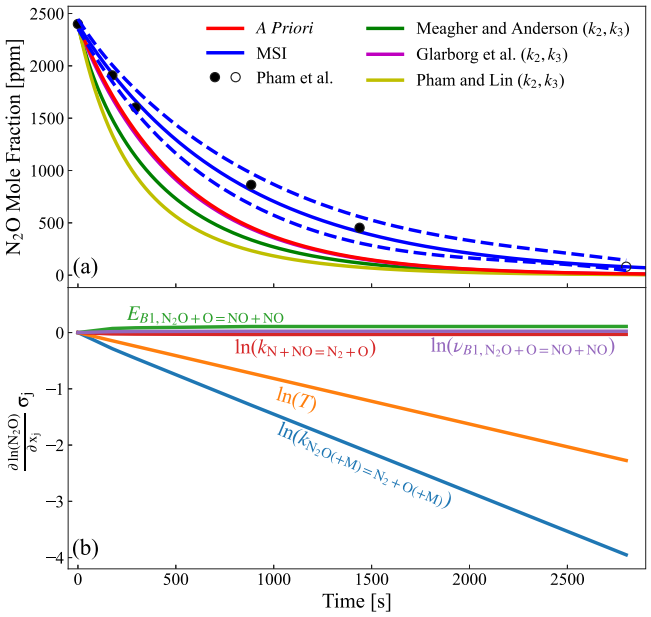

Fig. 6. (a) Time profiles and (b) corresponding uncertainty-weighted sensitivity coefficients for the N_2O mole fraction in a static reactor at 998 K and 1.053 atm for an initial mixture of 0.24% N_2O and Ar balance. Symbols denote experimental measurements of Pham et al. [17]; solid lines denote predictions using the *a priori* model, the MSI model, and variants of the *a priori* model that use k_2 and k_3 from [14,16,22]; dashed lines denote the propagated uncertainties in the MSI model predictions. (Note that the predictions using the *a priori* model and its variant with k_2 and k_3 from Glarborg et al. [22] are essentially indistinguishable).

cases (Figs. 1, S1, and 11) and better agreement for many cases (Figs. 2–6 and S2–S16). Given that k_1 in the MSI model is within ~20% of the *a priori* model (cf. Fig. 13), the small differences in many cases are not surprising. The slightly higher k_1 above ~1100 K and higher k_3 in the MSI model are consistent with the MSI model generally predicting faster rates of N_2O disappearance than the *a priori* model, which leads to better agreement with many experiments (Figs. 2–3 and S2–S16).

The much better agreement with the measured O time profiles of Ross et al. [25] (Figs. 4–5) and N_2O time profile of Pham et al. [17] (Fig. 6) appear to be primarily due to adjustments in the physical model parameters (the initial temperatures and O absorption cross sections), whose uncertainties are among the key contributors to prediction uncertainties (cf. bottom panels of Figs. 4 and 6). Specifically, the MSI model is able to better reproduce the data in Figs. 4, 5a, 5b, and 6 with adjustments to the O absorption coefficient by −6% from the nominal (reported) value and the initial temperatures by ~0.0%, −1.4%, 1.2%, and −1.2% from the (reported) nominal temperatures, respectively. For context, the reported O absorption coefficient from Ross et al. [25] was inferred from the data shown under the assumption that the final O mole fraction was equal to the initial N_2O mole fraction, which Fig. 4 suggests to be an inaccurate approximation. Likewise, the adjustments to the initial temperatures, which are within expected experimental uncertainties, would appear to explain the scatter in the observed rates (and derived k_1 values) in the experiments.

Fourth, the multi-species measurements of Allen et al. [36] (Fig. 1) and Haas et al. [43] (Fig. 11) also have important implications for reactions other than (R1). For example, uncertainty-weighted sensitivity analysis reveals that (R3), (R4), and (R5) (in addition to (R1)) are among the largest contributors to uncertainty in the predicted NO and NO_2 time profiles. While the MSI model maintains consistency with the N_2O time profiles, which are most directly informative of (R1), the MSI model is able to reproduce the measured NO and NO_2 profiles (including those of Allen et al. [36], with which the *a priori* model does not agree) via modest adjustments (within uncertainties) in the

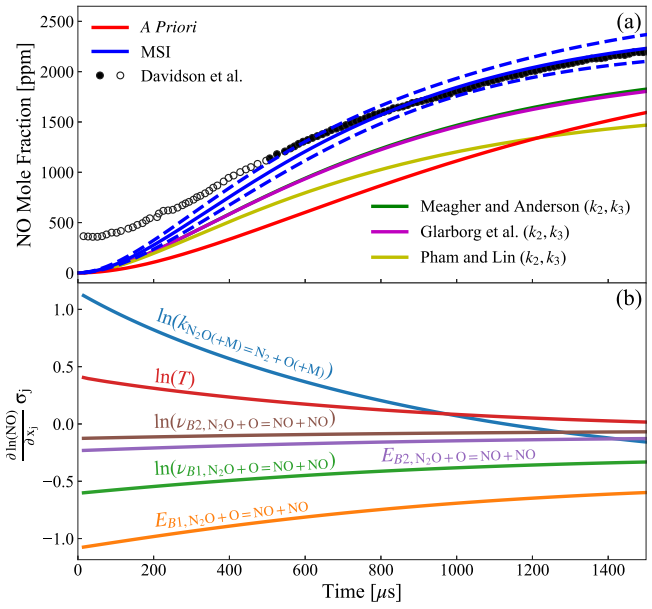

Fig. 7. (a) Time profiles and (b) corresponding uncertainty-weighted sensitivity coefficients for the NO mole fraction in a shock tube at 1868 K and 1.09 atm with an initial mixture of 0.535% N_2O and Ar balance. Symbols denote experimental measurements of Davidson et al. [23]; solid lines denote predictions using the *a priori* model, the MSI model, and variants of the *a priori* model that use k_2 and k_3 from [14,16,22]; dashed lines denote the propagated uncertainties in the MSI model predictions. Note that Davidson et al. [23] report that the experimental signals at early times are affected by N_2O interference and therefore do not yet reflect the NO mole fraction.

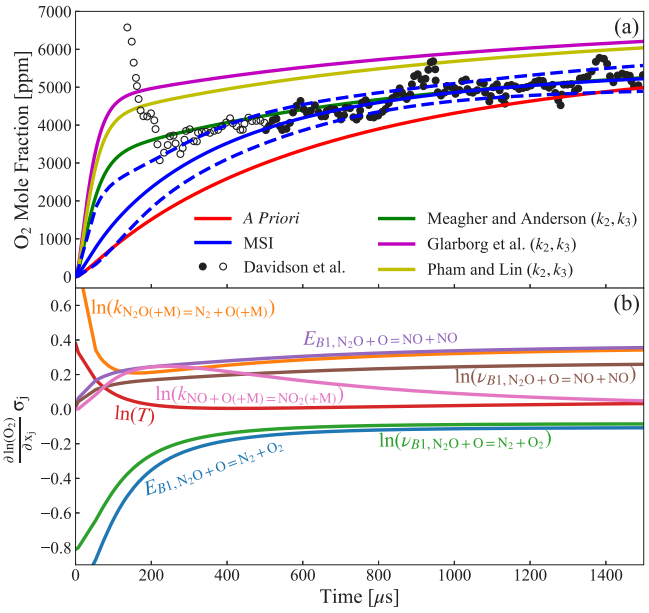

Fig. 8. (a) Time profiles and (b) corresponding uncertainty-weighted sensitivity coefficients for the O_2 mole fraction in a shock tube at 2268 K and 1.67 atm for an initial mixture of 2.34% N_2O and Ar balance. Symbols denote experimental measurements of Davidson et al. [23]; solid lines denote predictions using the *a priori* model, the MSI model, and variants of the *a priori* model that use k_2 and k_3 from [14,16,22]; dashed lines denote the propagated uncertainties in the MSI model predictions. Note that Davidson et al. [23] report that the experimental signals at early times are affected by N_2O interference and therefore do not yet reflect the NO mole fraction.

molecular parameters for (R3) (e.g., a 1 kcal/mol lower $E_{B1,R3}$ and 8% lower $\nu'_{B1,R3}$) and Arrhenius parameters for (R4) and (R5) that yield k_3, k_4, and k_5 in the MSI model that are, respectively, a factor of two, ~40%, and ~50% higher than the *a priori* model at 1173 K.

4.2. Experiments previously used to determine k_2 and k_3

This same MSI model is also shown to be consistent with the raw experimental data from several studies originally used to determine k_2 and k_3 in Figs. 7–12.

For example, Davidson et al. [23] used the measured NO time profiles in Fig. 7 for their k_3 determinations, which have been featured prominently in k_3 recommendations [14]. As noted in [23], the data at early times (<~0.5 ms) are impacted by interference due to broadband absorption by N_2O, such that only the datapoints after N_2O has decayed to negligible values actually reflect the NO mole fractions. The MSI model predictions reproduce the measured NO time profile [23] in Fig. 7 more closely than any other model, including those using k_3 expressions based on the k_3 determinations from Davidson et al. [23]—suggestive of secondary reactions influencing the derived k_3 values.

Indeed, Fig. 7b reveals significant uncertainty contributions from not only kinetic parameters related to k_3 but also k_1 and T (the initial temperature of the experiment)—implying that the time profiles constrain k_3 but in a manner coupled to k_1 and T. In this case, the MSI model improvements appear to be attributable to adjustments in all three sets of parameters, including molecular parameters for (R3) (discussed above) that yield a ~60% higher k_3, 20% higher k_1, and 1.9% higher T. Considering these other influences, the MSI model suggests an alternative interpretation of the data with a k_3 two times lower than originally derived [23].

Of even greater interest are the O_2 time profiles in Fig. 8 that Davidson et al. [23] used for their k_2 determinations, which first suggested a low pre-exponential factor and activation energy for k_2. After early times affected by N_2O interference (similar to the NO profiles), the MSI model reproduces the data more closely than models using k_2 and k_3 from González et al. [15] (i.e., the *a priori* model), Glarborg et al. [22], and Pham and Lin [16]; the MSI model also reproduces the data as well as the model using k_2 and k_3 from Meagher and Anderson [14].

Uncertainty-weighted sensitivity analysis for the O_2 time profile (Fig. 8b) using the MSI model notably reveals the largest influence of (R2) of all experimental data. However, uncertainties in the rate constants for three other reactions are equally, if not more, significant to experimental interpretations. In fact, while the influence of (R2) is large at the early times impacted by N_2O interference, its influence decays rapidly—such that, at later times, rate constants for (R1) and (R3) (the competitive channel) appear most influential. Consequently, the MSI model is able to reproduce the data just as well as the original interpretations [23] and the model employing k_2 and k_3 from Meagher and Anderson [14] with a k_2 that is nearly four times lower and, importantly, is also consistent with the theoretical calculations of González et al. [15] within uncertainties. For context, the modest improvements in the MSI model from those of the *a priori* model can be attributed to the adjustments to parameters for (R1), (R3), and (R4) (discussed above) along with a 2 kcal/mol lower $E_{B1,R2}$ and a 7% lower $\nu'_{B1,R2}$ that altogether yield a factor of two higher k_2(2268 K) than that of González et al. [15].

Together with k_2 originally derived [23] from the data in Fig. 8, the O fluorescence time profiles of Fontijn et al. [24] in Fig. 9 formed the basis for the k_2 recommendation from Meagher and Anderson [14]. In the experiments [24], photolysis of SO_2 in $N_2O/SO_2/Ar$ mixtures or O_2 in $N_2O/O_2/Ar$ mixtures produced O, for which microwave-induced fluorescence provided uncalibrated time-dependent signals. As noted in [24], thermal decomposition of N_2O in the experiments was significant, yielding a prominent background fluorescence signal of O (and, while not directly observable, addition of NO and NO_2 into the reactant mixture via (R3), (R4), and (R5)). Additionally, O atom loss via molecular diffusion was also significant [24]. To derive $k_2 + k_3$, Fontijn

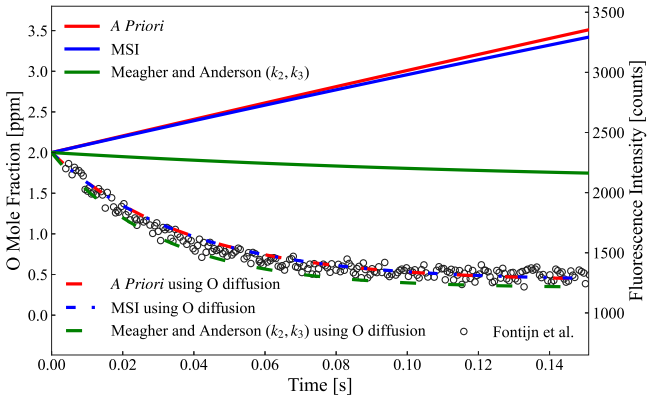

Fig. 9. Time profiles for the O mole fractions and fluorescence signals following photolysis to generate O atoms in a mixture predominantly composed of 0.13% N_2O and Ar balance at 1142 K and 1.313 atm. Symbols denote the uncalibrated fluorescence measurements of Fontijn et al. [24]; solid lines denote predictions without O atom diffusion using the *a priori* model, the MSI model, and the variant of the *a priori* model that uses k_2 and k_3 from Meagher and Anderson [14]; dashed lines denote predictions of the same models with O atom diffusion at the rate reported by Fontijn et al. [24] ($k_d = 26\ s^{-1}$).

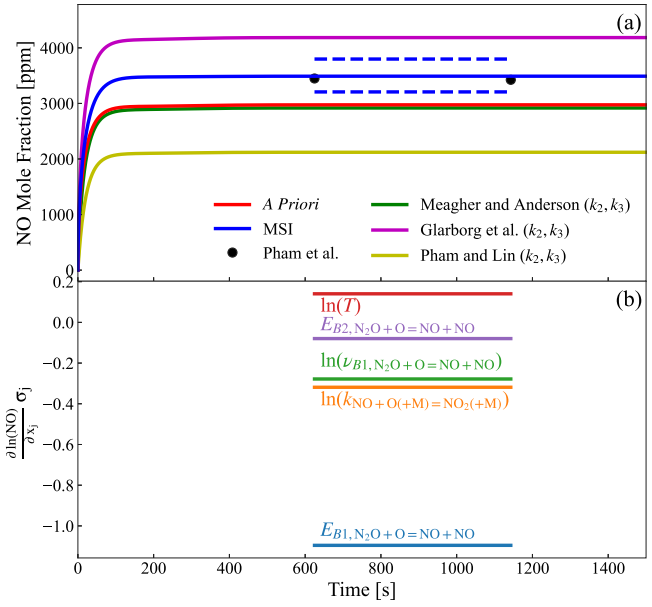

Fig. 10. (a) Time profiles and (b) corresponding uncertainty-weighted sensitivity coefficients for the NO mole fraction in a static reactor at 1083 K and 1.053 atm for an initial mixture of 7.1% N_2O and Ar balance. Symbols denote experimental measurements of Pham et al. [17]; solid lines denote predictions using the *a priori* model, the MSI model, and variants of the *a priori* model that use k_2 and k_3 from [14,16,22]; dashed lines denote the propagated uncertainties in the MSI model predictions.

et al. [24] fitted rates of exponential decay to their fluorescence time profiles and subtracted off estimated diffusion rates.

Interestingly, model predictions (without diffusion) using the *a priori* model, the MSI model, and the *a priori* model variant with k_2 and k_3 from Meagher and Anderson [14] are drastically different from each other and from the measured fluorescence signals (Fig. 9). However, model predictions using all three models that include a pseudo-first-order loss of O due to diffusion using the rate provided in [24] are nearly the same and all reproduce the fluorescence time profiles within the scatter of the data—despite using k_2 values that span four orders of magnitude.

Pham et al. [17] used the measured NO time profiles in Fig. 10 to determine k_2 values that were even five times higher than that of Meagher and Anderson [14]. Yet, the *a priori* model variant using k_2 and k_3 from Pham and Lin [16] does not reproduce the measurements, which indicates that the NO time profiles (similar to the N_2O profiles used by Pham et al. [17] to derive k_1) are sensitive to kinetic parameters for reactions other than the one derived from the data ((R2) in this case) and suggests an incompatibility among the rate constants in the model. Interestingly, the *a priori* model using a four-order-of-magnitude lower k_2 predicts NO time profiles that are only higher by ~50% than those predicted with k_2 from Pham and Lin [16] and already in reasonable agreement with the measurements.

While sensitivity analysis by Pham et al. [17] using their model (with a very high k_2 at 998 K) implied that their NO time profiles were most sensitive to k_2, sensitivity analysis (both uncertainty-weighted and conventional) using the MSI model indicates negligible sensitivity to k_2. The largest contributors to uncertainty evaluated with the MSI model are kinetic parameters for (R3) and (R4) and the initial temperature of the experiment (T), such that the modest improvements of the MSI model over the *a priori* model are largely due to the abovementioned adjustments to kinetic parameters for (R3) and (R4).

In another recent study, Haas et al. [43] used their measured N_2O, N_2, and NO time profiles to derive k_2/k_3 near 1000 K that also supported the higher ranges of proposed k_2. Similar to the comparisons of N_2O and N_2 time profiles discussed in Section 4.1, models with lower k_2 (MSI, *a priori*, and Glarborg et al. [22]) also reproduce the NO mole fractions well, whereas those with high k_2 (Meagher and Anderson [14] and Pham and Lin [16]) underpredict NO mole fractions (at least with the k_1 values in the *a priori* model). Uncertainty-weighted sensitivity analysis for the NO mole fractions of Haas et al. [43] (like those for Allen et al. [36] and Pham et al. [17]) reveal the influence of (R3) and (R4). MSI model predictions, which employ the abovementioned adjustments to kinetic parameters for (R3) and (R4) (that improved agreement with other NO data [17,36] in Figs. 1 and 10), still reproduce the NO data of Haas et al. [43] within uncertainties.

Finally, model predictions are compared with the measured outlet N_2O, N_2, O_2, NO, and NO_2 mole fractions from the jet-stirred reactor experiments of N_2O/NO_2/He mixtures from our companion study [37] in Fig. 12. As indicated by the model comparisons against the data shown in Fig. 12 (and the broader dataset in general, cf. [37]), models with high k_2 (Meagher and Anderson [14] and Pham and Lin [16]) systematically overpredict N_2 and O_2 and systematically underpredict NO; likewise, they underpredict outlet NO_2 for low inlet NO_2 (where NO_2 is produced on the net via (R3) and (R4)) and overpredict outlet NO_2 for high inlet NO_2 (where NO_2 is consumed on the net via (R5)). On the contrary, the MSI model reproduces the measurements for all species across all NO_2 inlet mole fractions with notable improvements over the *a priori* model attributable to the abovementioned adjustments to kinetic parameters for (R3), (R4), and (R5), which are among the most influential parameters identified by the (first-order) uncertainty-weighted sensitivity coefficients calculated with the MSI model (Fig. 12f–j). For reference, while predictions show little first-order sensitivity to k_2 for sufficiently low k_2 values (such as those of the *a priori* and MSI models), sensitivity to k_2 (and prediction error) increases rapidly with increasing k_2, such that very high k_2 [14,16] (regardless of rate constants for other reactions) are simply inconsistent with the data [37].

4.3. Rate constants

The rate constants of the MSI model are compared with those of the *a priori* model, previously proposed expressions [14,16,22], and the original experimental interpretations in Figs. 13–18. In general, the MSI rate constants are not the same as those originally derived from the data. That being said, as evident in Figs. 1–12, the MSI model reproduces the available raw data from the experimental studies just

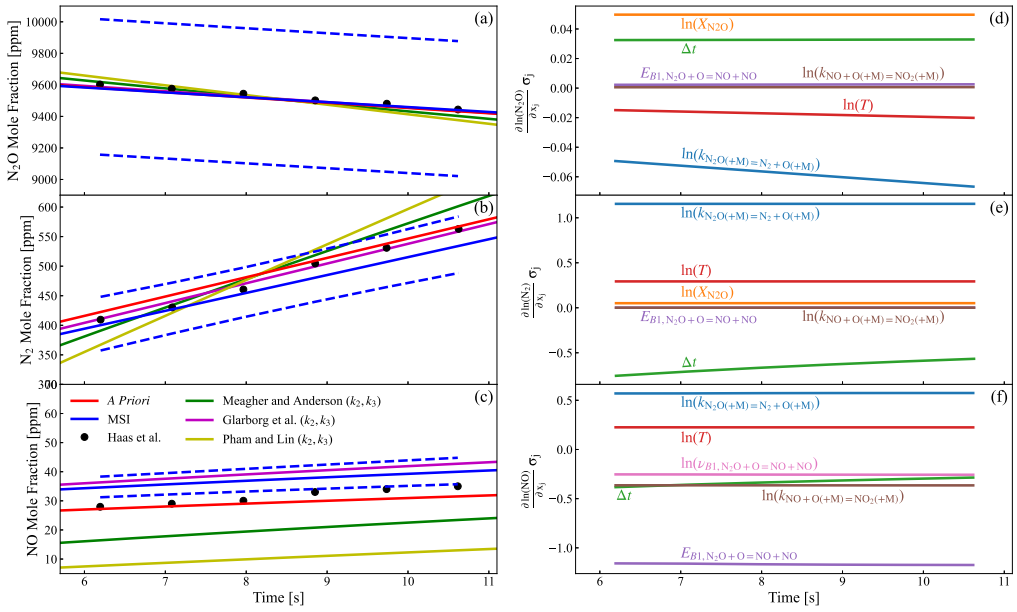

Fig. 11. Time profiles (a–c) and corresponding uncertainty-weighted sensitivity coefficients (d–f) for mole fractions of (a,d) N_2O, (b,e) N_2, and (c,f) NO in a flow reactor at 979 K and 4 atm for an initial mixture of 1.0% N_2O and Ar balance. Symbols denote experimental measurements of Haas et al. [43]; solid lines denote predictions using the *a priori* model, the MSI model, and variants of the *a priori* model that use k_2 and k_3 from [14,16,22]; dashed lines denote the propagated uncertainties in the MSI model predictions. All model predictions are time-shifted to yield the same N_2O mole fraction near the mid-point of N_2O consumption.

as well as the individual original interpretations—indicating that the present MSI interpretation is an equally valid interpretation of each isolated experiment.

However, the MSI model also achieves consistency across the broader theoretical and experimental dataset more holistically. These include the theoretical calculations of k_2 and k_3 from González et al. [15] and experimental determinations of k_4 and k_5. They also include a broad array of raw data originally used to determine k_1 [17,25,36,42,44,45] (Figs. 1–6 and S1–S16), as well as k_2 and k_3 [17,23,43] (Figs. 8–11), in addition to the new, uniquely informative measurements from Barbet et al. [37] (Fig. 12), which cannot be reproduced with high values of k_2 for any choices of rate constants for secondary reactions.

The most significant differences between the rate constants in the MSI model and those from previous experimental determinations and reviews are found for k_2 (Fig. 14) and k_2/k_3 (Fig. 16). Namely, k_2 in the MSI model is much lower than previous experimental determinations and recommendations at intermediate temperatures (by up to four orders of magnitude) and even somewhat lower (a factor of four or so) at higher temperatures. Yet, despite the many-orders-of-magnitude differences in k_2, $k_2 + k_3$, and k_2/k_3, the MSI model reproduces the raw data from the k_2 determinations of Davidson et al. [23] (Fig. 8) and Pham et al. [17] (Fig. 10), the $k_2 + k_3$ determinations of Fontijn et al. [24] (Fig. 9), and the k_2/k_3 determinations of Haas et al. [43] (Fig. 11) equally as well as the original interpretations.

Initially, the notion of reproducing the data with such drastically different k_2 may seem surprising. However, the influence of (R3), (R4), and (R5) in the MSI model predictions of these data (Figs. 8b, 10b, 11d–f) highlights the role of a catalytic sequence involving (R4) together with (R5) that systematically consumes O radicals and produces O_2. This sequence would tend to reduce the mole fraction of O, thereby reducing the NO yield from (R3), and inflate the O_2 yield—all of these factors would lead to an artificially high perceived k_2/k_3 (if interpreted in the absence of this sequence) as has been inferred previously. A further confounding factor is that the apparent role of this sequence depends on the rate parameters used in the local sensitivity analysis—such that a local sensitivity analysis employing larger values of k_2 (as performed in the original studies) would show large sensitivity to k_2 and much lower sensitivity to rate constants for secondary reactions.

Similarly, the significance of this sequence would not necessarily be apparent from even simultaneous measurements of multiple species during reaction of N_2O/diluent mixtures [36]. For example, Fig. 19a–e shows predictions of all five commonly measured species at conditions representative of previous experiments using the *a priori* model and a variant of it that uses k_2 from Meagher and Anderson [14] along with a 1.5 times higher k_1 and 2.9 times higher k_3 (which are within the range of literature values for k_1 [17,42] and k_3 [14,15,20,23]). As shown in Fig. 19a–e, the time profiles of all five species for the two models are nearly the same—despite their entirely different mechanistic descriptions (Fig. 19f–j)—and would probably be difficult to distinguish within experimental uncertainties.

In our MSI model, the values of k_2 are low enough relative to k_3 that the channel is completely insignificant for all but the highest temperatures. Only the O_2 time profiles of Davidson et al. [23] at 2268 K show any sensitivity to k_2. While the MSI model reproduces the O_2 time profiles at 2268 K with a factor of three lower k_2, the MSI model also shows a different temperature dependence from these k_2 determinations [23]. Of note, the interpretive uncertainties in the experimental O_2 profiles also depend on temperature. For example, while raw data are unavailable for temperatures other than 2268 K, N_2O interference was noted by Davidson et al. [23] to be larger at lower temperatures; and our uncertainty-weighted sensitivity analysis for the higher-temperature experiments reveal that uncertainties due to k_1 tend to increase substantially relative to those due to k_2.

One might also be suspicious of the impact of dissociation-induced depletion of high-energy N_2O states on the rate constants for its bimolecular reactions (R2) and (R3), a non-equilibrium effect only discovered recently [59]. Specifically, dissociation of N_2O at pressures less than the high-pressure limit leads to a well-known preferential depletion of high-energy N_2O molecules, which also can give rise to a historically unrecognized consequence [59]. Namely, since high-energy N_2O molecules would be expected to react more quickly than lower-energy N_2O molecules in bimolecular reactions with high activation

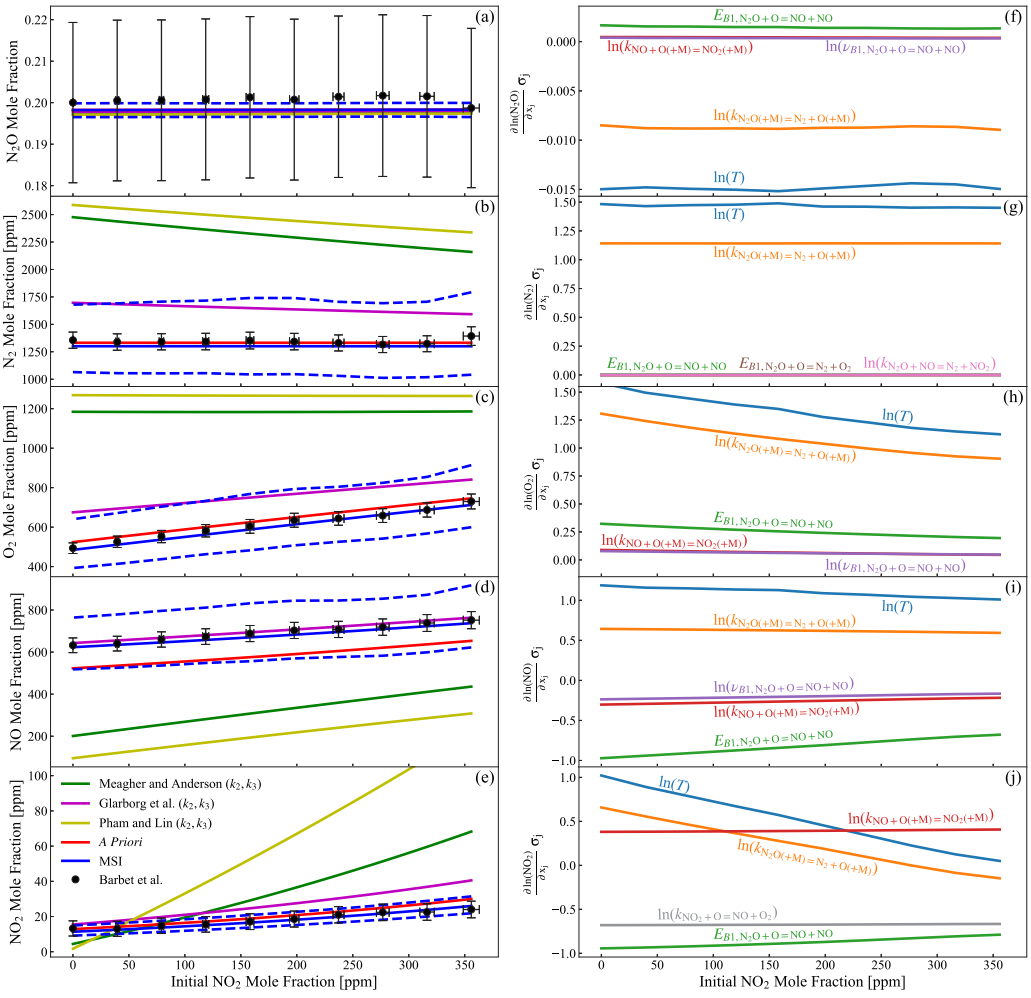

Fig. 12. Outlet mole fractions (a–e) and corresponding uncertainty-weighted sensitivity coefficients (f–j) for (a,f) N_2O, (b,g) N_2, (c,h) O_2, (d,i) NO, and (e,j) NO_2 in a jet-stirred reactor at 1050 K and 1.021 atm for a 0.45 s residence time and an inlet mixture of 20% N_2O, varied NO_2, and He balance. Symbols denote experimental measurements of Barbet et al. [37]; solid lines denote predictions using the *a priori* model, the MSI model, and variants of the *a priori* model that use k_2 and k_3 from [14,16,22]; dashed lines denote the propagated uncertainties in the MSI model predictions. (Note that all predictions of N_2O mole fraction in panel (a) are essentially indistinguishable).

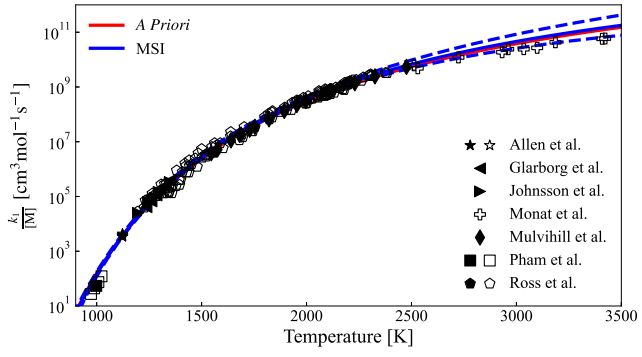

Fig. 13. Second-order rate constants for N_2O (+M) = N_2 + O (+M) (R1). Symbols denote the original experimental interpretations [17,25,36,42,44,45,55], where closed symbols specifically designate the original experimental determinations that correspond to the raw data shown in Figs. 1–6 and S1–S16 (where the MSI model reproduces the data); solid lines denote rate constants from the *a priori* model and MSI model (evaluated at 1 atm); dashed blue lines denote propagated uncertainties in the MSI model.

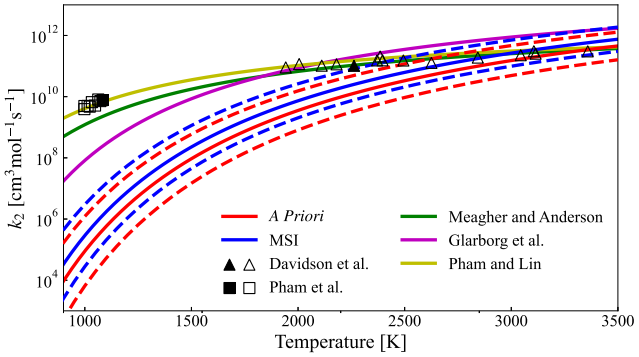

Fig. 14. Rate constants for N_2O + O = N_2 + O_2 (R2). Symbols denote the original experimental interpretations [17,23], where closed symbols specifically designate the original experimental determinations that correspond to the raw data shown in Figs. 8 and 10; solid lines denote rate constants from the *a priori* model, the MSI model, Meagher and Anderson [14], Glarborg et al. [22], and Pham and Lin [16]; dashed red and blue lines denote propagated uncertainties in the *a priori* model (i.e., the theoretical calculations of González et al. [15]) and the MSI model, respectively.

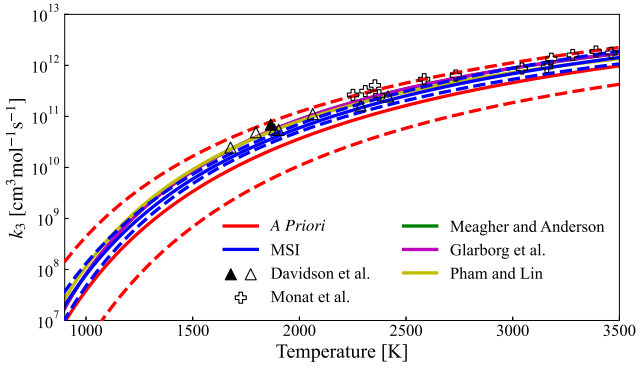

Fig. 15. Rate constants for $N_2O + O = NO + NO$ (R3). Symbols denote the original experimental interpretations [23,55], where closed symbols specifically designate the original experimental determinations that correspond to the raw data shown in Fig. 7; solid lines denote rate constants from the *a priori* model, the MSI model, Meagher and Anderson [14], Glarborg et al. [22], and Pham and Lin [16]; dashed red and blue lines denote propagated uncertainties in the *a priori* model (i.e., the theoretical calculations of González et al. [15]) and the MSI model, respectively.

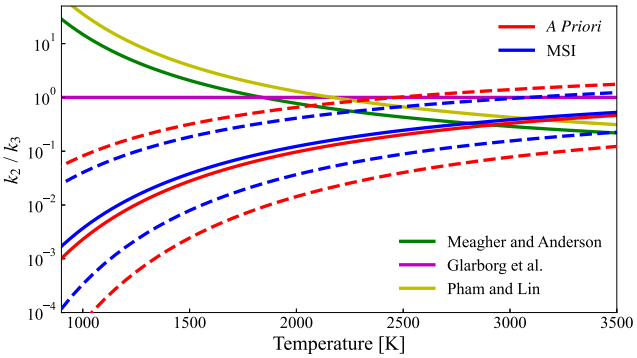

Fig. 16. Branching ratios for $N_2O + O$, k_2/k_3. Solid lines denote k_2/k_3 from the *a priori* model, the MSI model, Meagher and Anderson [14], Glarborg et al. [22], and Pham and Lin [16]; dashed red and blue lines denote propagated uncertainties in the *a priori* model (i.e., the theoretical calculations of González et al. [15]) and the MSI model, respectively.

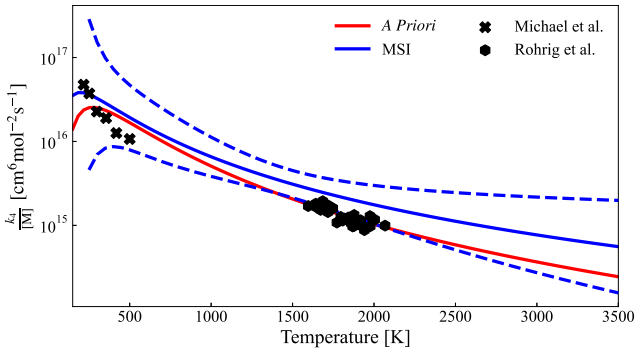

Fig. 17. Third-order rate constants for $NO + O (+M) = NO_2 (+M)$ (R4). Symbols denote the original experimental interpretations [49,50], for which no raw experimental data are available; solid lines denote rate constants from the *a priori* model and MSI model (evaluated at 1 atm); dashed blue lines denote propagated uncertainties in the MSI model.

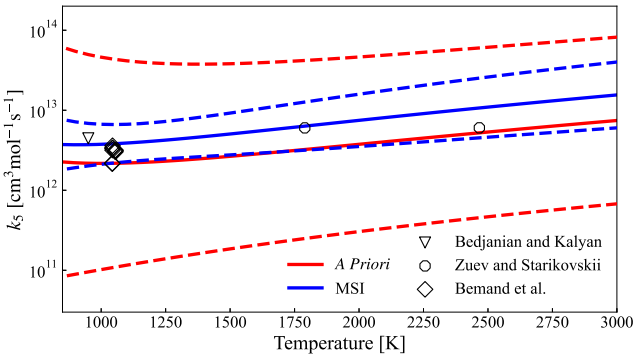

Fig. 18. Rate constants for $NO_2 + O = NO + O_2$ (R5). Symbols denote the original experimental interpretations [56–58]; solid lines denote rate constants from the *a priori* model and MSI model; dashed red and blue lines denote propagated uncertainties in the *a priori* model and the MSI model, respectively.

energy, the preferential depletion of high-energy N_2O states can lead to a reduction in bimolecular reaction rate constants from the typical thermal case, with greater reductions at higher temperatures. Preliminary calculations of this effect using a master equation for N_2O including collisional energy transfer, unimolecular dissociation to $O + N_2$, and bimolecular reaction with O via only the lowest transition state to form $N_2 + O_2$ (with a rate estimated by semi-microcanonical calculations) indicate that this effect may indeed complicate the temperature dependence of k_2 at high temperatures. Finite-pressure rate constants are found to be lower than thermal rate constants by less than 10% below 1500 K, by ~60% at 2268 K, and by a factor of four at 4000 K. With both the MSI and *a priori* models showing k_2/k_3 <~5 across all temperatures shown (even without accounting for this effect, which would be expected to be stronger for (R2) given its higher activation energy), dissociation-induced non-equilibrium at finite pressures may further reduce the k_2/k_3 and, likewise, reduce the relevance of the $N_2 + O_2$ channel at higher temperatures.

As a final note, the lack of (raw) data that are primarily sensitive to k_4 and k_5 at high temperatures or k_2 at any temperature precludes their rigorous, independent quantification. Consequently, posterior uncertainties for those rate constants remain quite large and the optimized values appear more dependent on the exact datasets and uncertainties used for inverse UQ. For example, if the O_2 time profiles of Fig. 8 (the only macroscopic observables where R2 is sensitive) are excluded from the target data used for inverse UQ, the MSI parameters and rate constants for R2 remain exactly at their prior values and rate constants for R4 remain closer to the prior values at higher temperatures. On a related note, the experiments of Fig. 8 involved higher reactant mole fractions (~2%) and commensurately higher temperature variations (~3%) than typical shock tube kinetics experiments and may be subject to additional uncertainties. Needless to say, improved quantification of the rate constants within the model would benefit from further theoretical calculations and/or experimental measurements, particularly at high temperatures.

5. Conclusions

A vast catalog of experimental and theoretical data for the reactions involved in N_2O decomposition [15,17,23–25,36,37,42–45] were analyzed using the MultiScale Informatics (MSI) approach. Overall, the resulting MSI model was shown to be consistent with all theoretical and raw experimental data within uncertainties (Figs. 1–12 and S1–S16), despite having rate constants for key reactions that differed substantially—sometimes by many orders of magnitude—from those originally derived from the same raw experimental data.

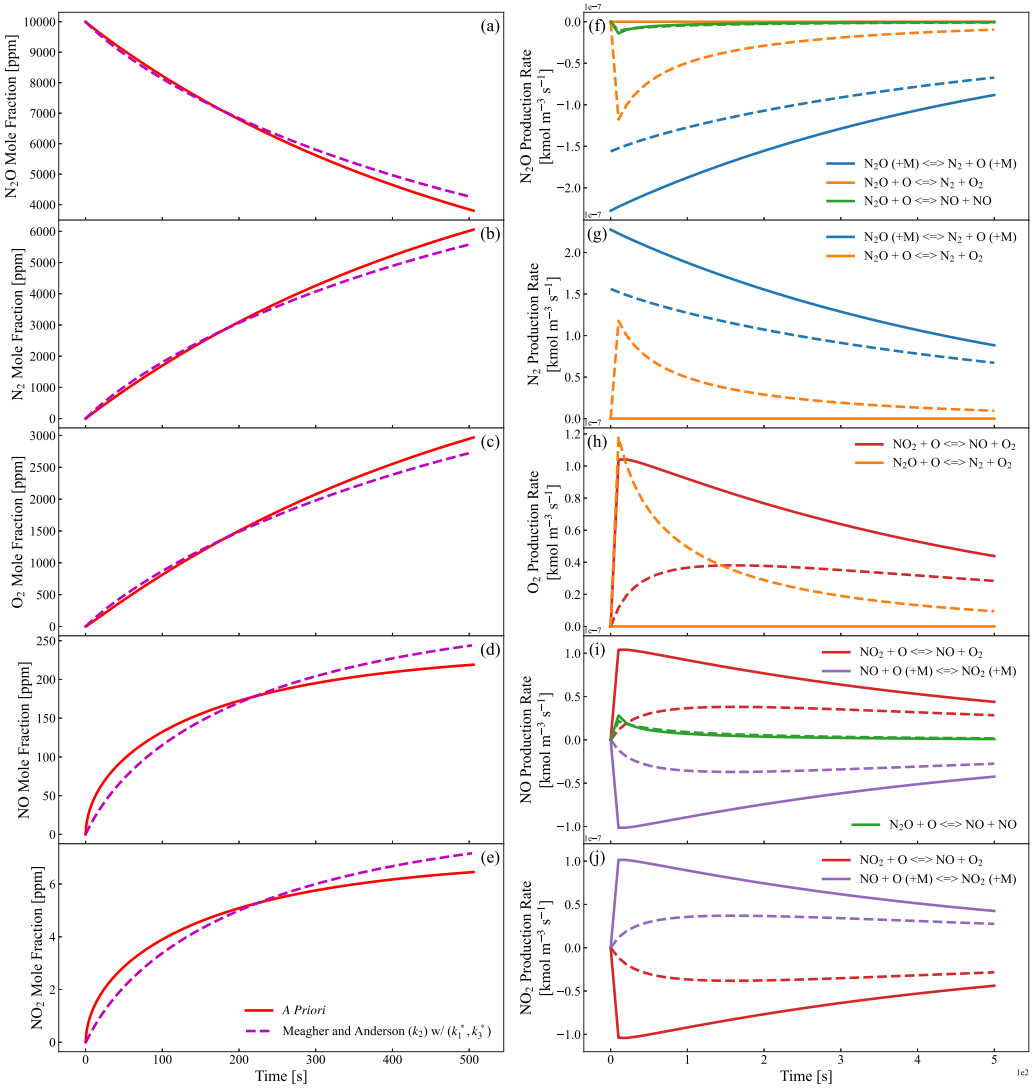

Fig. 19. Predicted time profiles (a–e) and corresponding production rates (f–j) of (a,f) N_2O, (b,g) N_2, (c,h) O_2, (d,i) NO, and (e,j) NO_2 for an initial mixture of 1% N_2O and Ar balance at 1000 K and 1 atm. Solid lines denote predictions of the *a priori* model and dashed lines denote predictions using a variant of the *a priori* model that employs k_2 from Meagher and Anderson [14] along with a 1.5 times higher k_1 and 2.9 times higher k_3 (which are within the range of literature values for k_1 [17,42] and k_3 [14,15,20,23]).

Of particular interest are the results for the $N_2O + O$ reaction—$N_2O + O = N_2 + O_2$ (R2) and $N_2O + O = NO + NO$ (R3)—whose branching ratio has been subject to considerable controversy. Notably, the present MSI model is consistent with both the theoretical calculations of González et al. [15] that show very low k_2 (and k_2/k_3) *and* the measured macroscopic observables from Davidson et al. [23], Fontijn et al. [24], Pham et al. [17], and Haas et al. [43] that previously anchored the very high proposed k_2 expressions [14,16,23]. This MSI model is also consistent with our new optimally designed experiments (from our companion paper [37]), which convincingly rule out the high k_2 values [14,16,23].

Further analysis conducted using this MSI model indicates the role of several secondary reactions in the experimental interpretations, including a catalytic sequence of reactions that consumes O and produces O_2. This sequence may have artificially inflated the apparent k_2/k_3 ratio previously deduced from experiments in a manner that may not have been detectable from even multi-species measurements at typical conditions—and may, therefore, explain the persistent historical difficulties in establishing the main products of $N_2O + O$.

Altogether, the present analysis along with the experimental measurements presented in our companion paper indicates that k_2 is sufficiently slow that NO + NO are the main products of $N_2O + O$ at essentially all temperatures.

CRediT authorship contribution statement

Joe Lee: Writing – review & editing, Writing – original draft, Software, Investigation, Formal analysis, Data curation. **Mark C. Barbet:** Writing – original draft, Investigation, Data curation, Conceptualization. **Carly E. LaGrotta:** Software. **Qinghui Meng:** Data curation. **Lei Lei:** Software, Data curation. **Francis M. Haas:** Writing – review & editing, Conceptualization. **Michael P. Burke:** Writing – review & editing, Writing – original draft, Supervision, Resources, Project administration, Funding acquisition, Conceptualization.

Declaration of competing interest

The authors declare that they have no known competing financial interests or personal relationships that could have appeared to influence the work reported in this paper.

Acknowledgments

The authors gratefully acknowledge support of this research by the National Science Foundation Combustion and Fire Systems program (CBET-1944004). The authors also thank Stephen Klippenstein for useful discussions.

Appendix A. Supplementary data

Supplementary material related to this article can be found online at https://doi.org/10.1016/j.combustflame.2024.113563.

References

[1] A. Durocher, G. Bourque, J.M. Bergthorson, Quantifying the effect of kinetic uncertainties on NO predictions at engine-relevant pressures in premixed methane–air flames, in: Proc. ASME Turbo Expo, Vol. 142, 2019, 061008.

[2] S.M. Correa, A review of NO_x formation under gas-turbine combustion conditions, Combust. Sci. Technol. 87 (1993) 329–362.

[3] P. Versailles, A. Durocher, G. Bourque, J.M. Bergthorson, Nitric oxide formation in lean, methane-air stagnation flames at supra-atmospheric pressures, Proc. Combust. Inst. 37 (2018) 711–718.

[4] W.R. Anderson, N.E. Meagher, J.A. Vanderhoff, Dark zones of solid propellant flames: Critically assessed datasets, quantitative model comparison, and detailed chemical analysis, Combust. Flame 158 (2011) 1228–1244.

[5] R.E. Cornell, M.C. Barbet, M.P. Burke, Automated discovery of influential chemically termolecular reactions in energetic material combustion: A case study for RDX, Proc. Combust. Inst. (2021) 787–794.

[6] P. Glarborg, J.S. Allingham, A.B. Skov, H. Hashemi, P. Marshall, Re-examination of the N_2O + O reaction, J. Phys. Chem. A 127 (2023) 6521–6531.

[7] C.R. Mulvihill, Y. Georgievskii, S.J. Klippenstein, Quantum and anharmonic effects in non-adiabatic transition state theory, J. Chem. Phys. 159 (2023) 174104.

[8] C.R. Mulvihill, Y. Georgievski, S.J. Klippenstein, Improvements to non-adiabatic statistical theories: Application to N_2O decomposition, in: 13th U.S. Natl. Combust. Meeting, 2023, paper 2A01.

[9] M.C. Barbet, M.P. Burke, Impact of "missing" third-body efficiencies on kinetic model predictions of combustion properties, Proc. Combust. Inst. 38 (2021) 425–432.

[10] A.W. Jasper, Predicting third-body collision efficiencies for water and other polyatomic baths, Faraday Discuss. 238 (2022) 68–86.

[11] L. Lei, M.P. Burke, Bath gas mixture effects on multichannel reactions: Insights and representations for systems beyond single-channel reactions, J. Phys. Chem. A 123 (2019) 631–649.

[12] L. Lei, M.P. Burke, Evaluating mixture rules and combustion implications for multi-component pressure dependence of allyl + HO_2 reactions, Proc. Combust. Inst. 37 (2019) 355–362.

[13] L. Lei, M.P. Burke, Dynamically evaluating mixture effects on multi-channel reactions in flames: A case study for the CH_3 + OH reaction, Proc. Combust. Inst. 38 (2021) 433–440.

[14] N.E. Meagher, W.R. Anderson, Kinetics of the $O(^3P)$ + N_2O reaction. 2. Interpretation and recommended rate coefficients, J. Phys. Chem. A 104 (2000) 6013–6031.

[15] M. González, R. Valero, R. Sayós, Ab initio ground potential energy surface ($^3A''$) for the $O(^3P)$ + N_2O reaction and kinetics study, J. Chem. Phys. 115 (2001) 2540–2549.

[16] T.V. Pham, M.C. Lin, Investigation of product formation in the $O(^1D, ^3P)$ + N_2O reactions: Comparison of experimental and theoretical kinetics, J. Phys. Chem. A 126 (2022) 1103–1113.

[17] T.V. Pham, T.J. Tsay, M.C. Lin, Thermal decomposition of N_2O near 900 K studied by FTIR spectrometry: Comparison of experimental and theoretical $O(^3P)$ formation kinetics, Int. J. Chem. Kinet. 52 (2020) 632–644.

[18] F. Kaufman, N.J. Gerri, R.E. Bowman, Role of nitric oxide in the thermal decomposition of nitrous oxide, J. Chem. Phys. 25 (1956) 106–115.

[19] R.K. Hanson, S. Salimian, Survey of rate constants in the N/H/O system, in: W.C. Gardiner (Ed.), Combustion Chemistry, Springer-Verlag, New York, 1984, pp. 361–422.

[20] D.L. Baulch, D.D. Drysdale, D.G. Horne, A.C. Lloyd, Evaluated Kinetic Data for High Temperature Reactions, vol. 2, The Butterworth Group, London, 1973.

[21] W. Tsang, J.T. Herron, Chemical kinetic data base for propellant combustion I. Reactions involving NO, NO_2, HNO, HNO_2, HCN and N_2O, J. Phys. Chem. Ref. Data 20 (1991) 609–663.

[22] P. Glarborg, J.A. Miller, B. Ruscic, S.J. Klippenstein, Modeling nitrogen chemistry in combustion, Prog. Energy Combust. Sci. 67 (2018) 31–68.

[23] D.F. Davidson, M.D. DiRosa, A.Y. Chang, R.K. Hanson, Shock tube measurements of the major product channels of N_2O + O, Shock Waves 2 (1992) 813–818.

[24] A. Fontijn, A. Goumri, A. Fernandez, W.R. Anderson, N.E. Meagher, Kinetics of the $O(^3P)$ + N_2O reaction. 1. Direct measurements at intermediate temperatures, J. Phys. Chem. A 104 (2000) 6003–6012.

[25] S.K. Ross, J.W. Sutherland, S.C. Kuo, R.B. Klemm, Rate constants for the thermal dissociation of N_2O and the $O(^3P)$ + N_2O reaction, J. Phys. Chem. A 101 (1997) 1104–1116.

[26] Y. Zhang, O. Mathieu, E.L. Petersen, G. Bourque, H.J. Curran, Assessing the predictions of a NO_x kinetic mechanism on recent hydrogen and syngas experimental data, Combust. Flame 182 (2017) 122–141.

[27] N. Lamoureux, H.E. Merhubi, L. Pillier, S. de Persis, P. Desgroux, Modeling of NO formation in low pressure premixed flames, Combust. Flame 163 (2016) 557–575.

[28] S.J. Klippenstein, L.B. Harding, P. Glarborg, J.A. Miller, The role of NNH in NO formation and control, Combust. Flame 158 (2011) 774–789.

[29] A.M. Dean, J.W. Bozzelli, Combustion chemistry of nitrogen, in: W.C. Gardiner (Ed.), Gas-Phase Combustion Chemistry, Springer New York, New York, NY, 2000, pp. 125–341.

[30] G.P. Smith, D.M. Golden, M. Frenklach, N.W. Moriarty, B. Eiteneer, M. Goldenberg, C.T. Bowman, R.K. Hanson, S. Song, W.C. Gardiner Jr., V. Lissianski, Z. Qin, GRI-Mech 3.0.

[31] X. Han, M.L. Lavadera, A.A. Konnov, An experimental and kinetic modeling study on the laminar burning velocity of NH_3 + N_2O + air flames, Combust. Flame 228 (2021) 13–28.

[32] K.P. Shrestha, L. Seidel, T. Zeuch, F. Mauss, Detailed kinetic mechanism for the oxidation of ammonia including the formation and reduction of nitrogen oxides, Energy Fuels 32 (2018) 10202–10217.

[33] J. Otomo, M. Koshi, T. Mitsumori, H. Iwasaki, K. Yamada, Chemical kinetic modeling of ammonia oxidation with improved reaction mechanism for ammonia/air and ammonia/hydrogen/air combustion, Int. J. Hydrog. Energy 43 (2018) 3004–3014.

[34] A. Stagni, C. Cavallotti, S. Arunthanayothin, Y. Song, O. Herbinet, F. Battin-Leclerc, T. Faravelli, An experimental, theoretical and kinetic-modeling study of the gas-phase oxidation of ammonia, React. Chem. Eng. 5 (2020) 696–711.

[35] A.P. Zuev, A.Y. Starikovskii, Reactions involving nitrogen oxides at high temperature. Reactions of N_2O with atomic oxygen, Sov. J. Chem. Phys. 10 (1992) 255–272.

[36] M.T. Allen, R.A. Yetter, F.L. Dryer, The decomposition of nitrous oxide at $1.5 \leq P \leq 10.5$ atm and $1103 \leq T \leq 1173$ K, Int. J. Chem. Kinet. 27 (1995) 883–909.

[37] M.C. Barbet, J. Lee, C.E. LaGrotta, R.E. Cornell, M.P. Burke, An experimental platform for semi-autonomous kinetic model refinement combining optimal experimental design, computer-controlled experiments, and optimization leads to new understanding of N_2O + O, Combust. Flame (2023) http://dx.doi.org/10.1016/j.combustflame.2024.113562, In press.

[38] M.P. Burke, Harnessing the combined power of theoretical and experimental data through multiscale informatics, Int. J. Chem. Kinet. 48 (2016) 212–235.

[39] C.E. LaGrotta, M.C. Barbet, L. Lei, M.P. Burke, Towards a high-accuracy kinetic database informed by theoretical and experimental data: CH_3 + HO_2 as a case study, Proc. Combust. Inst. 38 (2021) 1043–1051.

[40] C.E. LaGrotta, Q. Meng, L. Lei, M.C. Barbet, Z. Hong, M.P. Burke, Resolving discrepancies between state-of-the-art theory and experiment for HO_2 + HO_2 via multiscale informatics, J. Phys. Chem. A 127 (2023) 799–816.

[41] Y. Li, S. Javoy, R. Mevel, X. Xu, A chemically consistent rate constant for the reaction of nitrogen dioxide with the oxygen atom, Phys. Chem. Chem. Phys. 23 (2021) 585–596.

[42] P. Glarborg, J.E. Johnsson, K. Dam-Johansen, Kinetics of homogeneous nitrous oxide decomposition, Combust. Flame 99 (1994) 523–532.

[43] F.M. Haas, F.E. Alam, J.S. Santner, T.I. Farouk, F.L. Dryer, Branching ratio of N_2O + O → products determined from flow reactor experiments at intermediate temperatures, in: 11th U.S. Natl. Combust. Meeting, 2019, paper 3A03.

[44] J.E. Johnsson, P. Glarborg, K. Dam-Johansen, Thermal dissociation of nitrous oxide at medium temperatures, Symp. (Int.) Combust. 24 (1992) 917–923.

[45] C.R. Mulvihill, S.A. Alturaifi, E.L. Petersen, A shock-tube study of the N_2O + M ⇌ N_2 + O + M (M = Ar) rate constant using N_2O laser absorption near 4.6 μm, Combust. Flame 224 (2020) 6–13.

[46] H. Wang, D.A. Sheen, Combustion kinetic model uncertainty quantification, propagation and minimization, Prog. Energy Combust. Sci. 47 (2015) 1–31.

[47] G.P. Smith, Y. Tao, H. Wang, Foundational fuel chemistry model version 1.0 (FFCM-1.0), 2016.

[48] C. Olm, T. Varga, É. Valkó, H.J. Curran, T. Turányi, Uncertainty quantification of a newly optimized methanol and formaldehyde combustion mechanism, Combust. Flame 186 (2017) 45–64.

[49] M. Röhrig, E.L. Petersen, D.F. Davidson, R.K. Hanson, A shock tube study of the pyrolysis of NO_2, Int. J. Chem. Kinet. 29 (1997) 483–493.

[50] J.V. Michael, W.A. Payne, D.A. Whytock, Absolute rate constants for O + NO + M (=He, Ne, Ar, Kr) → NO_2 + M from 217–500 K, J. Chem. Phys. 65 (1976) 4830–4834.

[51] R.E. Cornell, M.C. Barbet, J. Lee, M.P. Burke, NH_3 oxidation by NO_2 in a jet-stirred reactor: The effect of significant uncertainties in H_2NO kinetics, Appl. Energy Combust. Sci. 12 (2022) 100095.

[52] D.A. Masten, R.K. Hanson, C.T. Bowman, Shock tube study of the reaction H + O_2 → OH + O using OH laser absorption, J. Phys. Chem. 94 (1990) 7119–7128.

[53] F.L. Dryer, F.M. Haas, J. Santner, T.I. Farouk, M. Chaos, Interpreting chemical kinetics from complex reaction–advection–diffusion systems: Modeling of flow reactors and related experiments, Prog. Energy Combust. Sci. 44 (2014) 19–39.

[54] D.G. Goodwin, H.K. Moffat, R.L. Speth, Cantera: An object-oriented software toolkit for chemical kinetics, thermodynamics, and transport processes, 2017, Version 2.5.1.

[55] J.P. Monat, R.K. Hanson, C.H. Kruger, Kinetics of homogeneous nitrous oxide decomposition, Combust. Sci. Technol. 16 (1977) 21–28.

[56] P.P. Bemand, M.A.A. Clyne, R.T. Watson, Atomic resonance fluorescence and mass spectrometry for measurements of the rate constants for elementary reactions: $O(^3P) + NO_2 \rightarrow NO + O_2$ and $NO + O_3 \rightarrow NO_2 + O_2$, J. Chem. Soc. Faraday Trans. 2 70 (1974) 564–576.

[57] Y. Bedjanian, C. Kalyan, Rate constants of the reactions of $O(^3P)$ atoms with Br_2 and NO_2 over the temperature range 220–950 K, Int. J. Chem. Kinet. 51 (2019) 476–483.

[58] A.P. Zuev, A.Y. Starikovskii, Reactions involving nitrogen oxides at high temperature. The reactions of $NO + O + M \rightarrow NO_2 + M$ and $NO_2 + O \rightarrow NO + O_2$, Khim. Fiz. 10 (1991) 190–199.

[59] M.P. Burke, Q. Meng, C. Sabaitis, Dissociation-induced depletion of high-energy reactant molecules as a mechanism for pressure-dependent rate constants for bimolecular reactions, Faraday Discuss. 238 (2022) 355–379.